Fast-ion transport in $q_{min} > 2$, high-β steady-state scenarios on DIII-D[a)]

C. T. Holcomb,[1,b)] W. W. Heidbrink,[2] J. R. Ferron,[3] M. A. Van Zeeland,[3] A. M. Garofalo,[3] W. M. Solomon,[4] X. Gong,[5] D. Mueller,[4] B. Grierson,[4] E. M. Bass,[3] C. Collins,[2] J. M. Park,[6] K. Kim,[6] T. C. Luce,[3] F. Turco,[7] D. C. Pace,[3] Q. Ren,[5] and M. Podesta[4]
[1]*Lawrence Livermore National Laboratory, Livermore, California 94551, USA*
[2]*Department of Physics and Astronomy, University of California Irvine, Irvine, California 92697, USA*
[3]*General Atomics, P.O. Box 85608, San Diego, California 92186-5608, USA*
[4]*Princeton Plasma Physics Laboratory, P.O. Box 451, Princeton, New Jersey 05843, USA*
[5]*Institute of Plasma Physics, Chinese Academy of Sciences, Hefei, Anhui 230031, China*
[6]*Oak Ridge National Laboratory, P.O. Box 2008, Oak Ridge, Tennessee 37831, USA*
[7]*Columbia University, 2960 Broadway, New York, New York 10027, USA*

(Received 5 January 2015; accepted 17 April 2015; published online 22 May 2015)

Results from experiments on DIII-D [J. L. Luxon, Fusion Sci. Technol. **48**, 828 (2005)] aimed at developing high β steady-state operating scenarios with high-q_{min} confirm that fast-ion transport is a critical issue for advanced tokamak development using neutral beam injection current drive. In DIII-D, greater than 11 MW of neutral beam heating power is applied with the intent of maximizing β_N and the noninductive current drive. However, in scenarios with $q_{min} > 2$ that target the typical range of $q_{95} = 5$–7 used in next-step steady-state reactor models, Alfvén eigenmodes cause greater fast-ion transport than classical models predict. This enhanced transport reduces the absorbed neutral beam heating power and current drive and limits the achievable β_N. In contrast, similar plasmas except with q_{min} just above 1 have approximately classical fast-ion transport. Experiments that take $q_{min} > 3$ plasmas to higher β_P with $q_{95} = 11$–12 for testing long pulse operation exhibit regimes of better than expected thermal confinement. Compared to the standard high-q_{min} scenario, the high β_P cases have shorter slowing-down time and lower $\nabla\beta_{fast}$, and this reduces the drive for Alfvénic modes, yielding nearly classical fast-ion transport, high values of normalized confinement, β_N, and noninductive current fraction. These results suggest DIII-D might obtain better performance in lower-q_{95}, high-q_{min} plasmas using broader neutral beam heating profiles and increased direct electron heating power to lower the drive for Alfvén eigenmodes. [http://dx.doi.org/10.1063/1.4921152]

I. INTRODUCTION

Understanding superthermal fast-ion transport caused by interaction with Alfvén eigenmodes (AEs) is an important aspect of steady-state scenario development in existing tokamaks heated by neutral beam injection (NBI). The DIII-D program is testing a range of potential high-β, fully noninductive operating scenarios for next-step long pulse tokamaks leading up to the development of a fusion power plant. Primarily, the shape of the current density profile distinguishes the scenarios from each other, and this ranges from strongly peaked to very hollow. Access to this range of profiles is provided by adjustable NBI and electron cyclotron heating (ECH) and current drive (ECCD).[1]

Presently and for the near future, the available NBI power on DIII-D is at least 3 times greater than the available ECH power, so most high-β scenario exploration is dominated by NBI power. In such cases, the classically predicted β_{fast} can approach ~40% of β_{total}. Low-density operation is often chosen, because this is expected to maximize the noninductive current drive.[2] There are plans to increase both the NBI and ECH power, including more off-axis NBI. The classical fast-ion slowing down time on thermal electrons is proportional to $T_e^{3/2}/n_e$, where T_e is the electron temperature and n_e is the density.[3] If significant increases in NBI and ECH power were applied to future plasmas then the classical slowing-down time would increase, especially at low density, and the classically predicted fast-ion fraction $\beta_{fast}/\beta_{total}$ could increase. Such changes would increase the possibility for interaction between fast-ions and AEs. This may cause enhanced (i.e., higher than classical prediction) fast-ion transport that may take the form of redistribution to higher radius or loss to the wall. Enhanced fast-ion transport can reduce the power that would otherwise be absorbed by the thermal plasma, and it can reduce or redistribute the NBI current drive.[4] Therefore, understanding how candidate steady-state operating scenarios can affect the drive and damping of fast-ion modes is essential.

The prototypical high-β steady-state scenario envisioned for many future devices uses an elevated q-profile. Various ITER steady state scenario models have $q_{min} > 2$ with β_N near 2.5–3.[5,6] A Fusion Nuclear Science Facility design (FNSF-AT) uses $q_{min} > 1.4$ with strong negative central shear at $\beta_N = 3.7$.[7] The ARIES-AT design uses $q_{min} = 2.4$ and $\beta_N = 5.4$.[8] All of these designs are based on several predicted advantages for steady-state operation at high q_{min}. These include (i) a high ideal-wall kink mode β limit when the current density is sufficiently broad or hollow to produce strong coupling to a nearby conducting wall,[9] (ii) a high

[a)]Paper YI1 4, Bull. Am. Phys. Soc. **59**, 364 (2014).
[b)]Invited speaker.

bootstrap current fraction, which scales as β-poloidal (β_P) or $q\beta_N$,[10] (iii), avoidance of low-order tearing modes by exclusion of rational surfaces from the plasma, e.g., the $m/n = 2/1$ tearing mode when $q_{min} > 2$,[11] and (iv) thermal confinement exceeding typical H-mode levels enabled by weak or negative magnetic shear.[12]

Present experiments can test physics that goes into predictive models for next-step steady-state devices. For example, one can test if a proposed current profile is capable of sustaining the target value of β_N without encountering resistive tearing modes. Also of interest is whether or not the current profile is consistent with the expected transport and energy confinement.

Such questions motivated several experiments on DIII-D to identify β_N limits in steady-state scenario plasmas with q_{min} sustained above 2. The experiments identified unexpected 20%–30% differences in the normalized global energy confinement between two different regimes. Both regimes were tested with toroidal field 1.75–2.1 T, and in double-null shapes. The "standard high-q_{min}" regime has $q_{min} =$ 2–2.5, $q_{95} =$ 5–7, line-density $= 3.5–4.5 \times 10^{19}$ m^{-3}, $I_P =$ 0.8–1 MA, and Greenwald fraction[13] near 0.5. These conditions were chosen to target fully noninductive operation with a significant fraction of externally driven current, and projected fusion gain sufficient for next-step tokamaks like FNSF. In these plasmas, β_N is usually limited to about 3 by the available power, and the normalized global energy confinement H_{89P}[14] is typically 1.6–1.8.[15] A "high-β_P" regime developed for testing long-pulse operation on the EAST tokamak[16] has $q_{min} =$ 3–5, $q_{95} =$ 11–12, line-averaged density $= 5–6.5 \times 10^{19}$ m^{-3}, $I_P = 0.6–0.65$ MA, and Greenwald fraction near 1. β_N is limited to about 4 by instability rather than by confinement, and $H_{89P} = 2–3$.

This paper discusses measurements and modeling that confirm that differences in AE stability and enhanced fast-ion transport account for the observed large variation in normalized confinement. To summarize, in standard high-q_{min} plasmas many AEs are unstable across a majority of the plasma radius, and these lead to fast-ion transport greater than that predicted by classical theory. This limits the absorbed heating power and limits the achievable β_N. Similar plasmas having q_{min} just above 1 have less AE activity and approximately classical fast-ion transport. A detailed paper on fast-ion measurements in these discharges was recently published.[28] High-β_P plasmas have better than expected total energy confinement because of the presence of either a high-radius transport barrier or a high pedestal pressure. In these cases, the fast ion transport approaches the classical level. This is due to lower drive for AEs near the axis caused by a lower gradient in the fast ion pressure. These results suggest that increasing global confinement and β_N in high-q_{min} plasmas at lower q_{95} might be achieved by broadening the NBI and ECH heating profiles to reduce core AE activity, and further optimization of thermal transport.

II. COMPARISON OF HIGH- AND LOW-q_{min} DISCHARGES HAVING $q_{95} = 5–7$

The current density or q-profile is a key attribute of the equilibrium that may be adjusted to optimize steady-state operation and projected fusion power gain. Most potential steady-state scenarios tested on DIII-D for use in a next-step reactor have q_{95} in the range of 5–7 during the high-β_N phase of the discharge when the inductive current fraction is minimized. By adjusting the L-to-H-mode transition time and the starting time of high-power NBI and ECH, q_{min} during the high-β_N phase can be set to a value between ~1 and ~2.5. At the low end of this range are scenarios like the "high-l_i"[17] and "steady-state hybrid"[18] that have potential applicability in next-step reactors. These tend to have good total energy confinement, i.e., $H_{89P} \geq 2$, and approximately classical fast-ion confinement. This paper focuses on fast-ion transport in high-q_{min} plasmas, but comparison of similar high- and low-q_{min} plasmas serves to elucidate many of the effects.

Figure 1(a) compares the q-profiles obtained during the high-β_N phases of a pair of consecutive discharges. During the time range t = 3.2–3.7 s the case with $q_{min} \approx 1$ obtained $\beta_N = 2.9$ using 8 MW of NBI and 1.3 MW of ECH at $H_{89P} = 2.2$. During the same time period, the case with $q_{min} \approx 2$ obtained $\beta_N = 2.6$ using 9.4 MW of NBI and

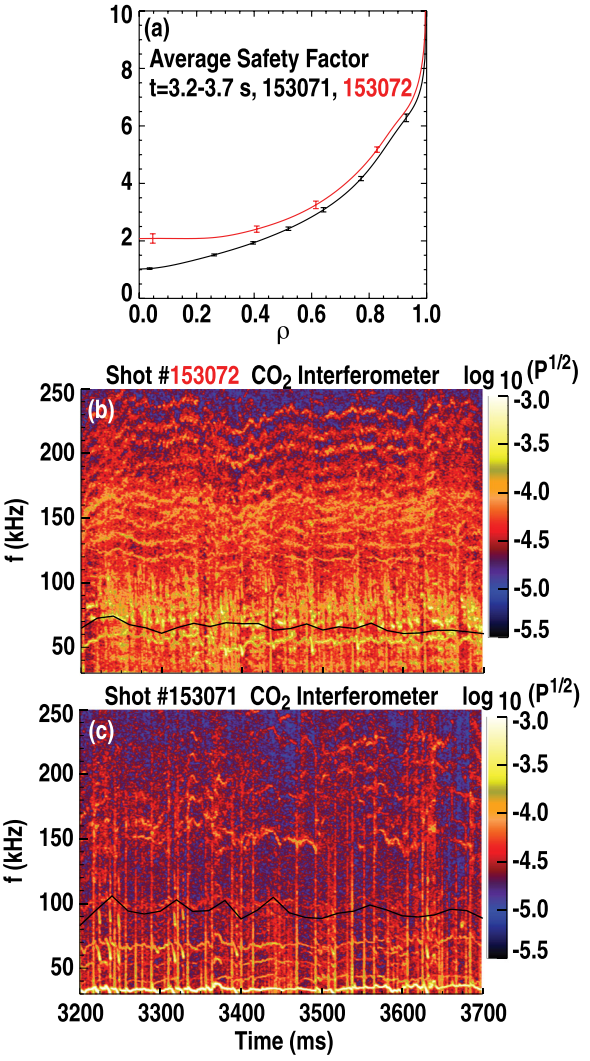

FIG. 1. (a) Safety factor profiles during the high-β_N phase of two discharges. (b) and (c) Cross-power density fluctuation spectra vs time from CO_2 interferometer chords showing AEs for the (b) high-q_{min} case and (c) low-q_{min} case. The solid black lines denote the TAE frequency at the magnetic axis.

1.3 MW of ECH at $H_{89P} = 1.8$. During the analysis time period, both discharges use the same boundary shape and have density profiles with the same shape, but the $q_{min} \approx 2$ case is about 10% lower density at all radii. The ion and electron temperature profiles outside $\rho = 0.5$ are the same within 10%, but inside $\rho = 0.5$ the $q_{min} \approx 2$ case has significantly lower temperature, i.e., 20% lower Te(0) and 25% lower Ti(0). Due to these differences, the $q_{min} \approx 2$ case has about a 20% shorter classical fast-ion slowing-down time at the magnetic axis than the $q_{min} \approx 1$ case. While a shorter on-axis slowing-down time might be expected to result in lower Alfvénic activity, the observations show otherwise. The cross-power density-fluctuation spectra between the two most central interferometer chords shows significantly more toroidal Alfvén eigenmode (TAE)[20] activity in the plasma with $q_{min} \approx 2$ than the plasma with $q_{min} \approx 1$ [Figs. 1(b) and 1(c)]. To quantify this, the average amplitude of coherent modes with frequency in the TAE frequency band[28] is about four times higher in the high-q_{min} plasma. A plastic scintillator neutron counter measured a ~43% lower signal in the high-q_{min} case compared to the low q_{min}-case.

The apparent correlation between higher AE activity, lower neutron rate, and lower normalized global energy confinement suggests that enhanced fast-ion transport could be a significant energy loss channel. All of the direct fast-ion loss detectors on DIII-D only work when $I_P > 0$ and $B_T < 0$ because this is the configuration used by most experiments. All experiments described in this paper use $I_P > 0$ and $B_T > 0$ to maximize the off-axis NBI current drive that helps maintain elevated q_{min}, and therefore no direct measurements of fast-ion loss exist. Instead, enhanced fast-ion transport above the classically predicted level is inferred by comparing two ways to compute the plasma total stored energy. First, the EFIT code[21] is used for equilibrium reconstructions by fitting to magnetic measurements outside the plasma. This method accurately determines the total stored energy W_{EFIT} to better than 3% over the range of β_P obtained in this study. This is based on a Monte-Carlo statistical analysis of magnetic reconstructions with a 3% uncertainty in external magnetic measurements as described in Sec. 3.2 of Ref. 21. The second method is to use the ONETWO transport code[22] to compute the total stored energy W_C, using the magnetic geometry, measured density and temperature profiles, and NBI power and injection angles as inputs. The NUBEAM Monte Carlo code[23] is used to compute the fast-ion distribution function assuming that the fast-ion transport is completely classical. NUBEAM does not account for possible neutral beam ionization in the scrape-off layer. This is estimated to be up to 3%–4% of the beam power depending on the scrape-off layer density. Figure 2 shows the values of W_{EFIT} and W_C determined from both approaches for the two discharges in Fig. 1. Figure 2(b) shows the percentage that W_C overestimates W_{EFIT}—a value that will be referred to as the "stored energy overestimate" throughout this paper. The plasma with $q_{min} \approx 1$ has good agreement between the measured and computed total stored energies—the average stored energy overestimate during the high β_N phase shown is 3%. Therefore, within the uncertainties, classical fast-ion transport is an accurate description for this plasma. In contrast the

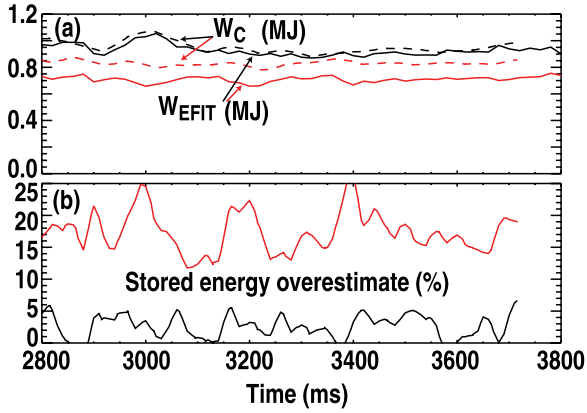

FIG. 2. (a) Comparison of W_C and W_{EFIT} vs time for the discharges shown in Fig. 1. (b) Stored energy overestimate defined as $(W_C - W_{EFIT})/W_{EFIT}$.

high-q_{min} case W_C overestimates W_{EFIT} by an average of 17%. This overestimate is interpreted as an indication of fast ion redistribution and/or loss.

Fast-ion D_α (FIDA) diagnostic measurements[24] confirm that high-q_{min} plasmas can have a deficit of fast ions compared to the level expected classically. Several FIDA views are available on DIII-D, but in steady-state scenario plasmas these do not routinely make useful measurements without careful design of the various NBI source waveforms. This must be done to provide background subtraction and temporally isolate "signal" beams the diagnostic is tuned to from "polluting" beams that it is not. This was done for the pair of discharges in Figs. 1 and 2. Figure 3 compares measurements from a vertical-viewing FIDA array with synthetic diagnostic predictions using the FIDASIM code.[25] The solid lines are the FIDASIM predictions for the high- and low-q_{min} cases using a classical fast-ion transport assumption. The classical prediction for the high-q_{min} case exceeds that of the low-q_{min} case. However, the FIDA measurements are at approximately the same level for both cases, so that the classical prediction roughly matches most measurements for $q_{min} \approx 1$, but the classical prediction is higher than the measurements for $q_{min} \approx 2$. The dashed line is the FIDASIM prediction for the $q_{min} \approx 2$ case after applying an ad-hoc uniform fast-ion

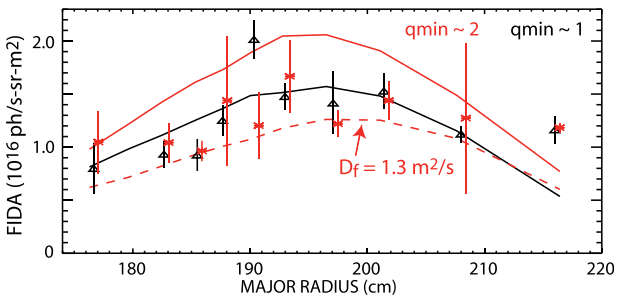

FIG. 3. Plot of fast-ion brightness (proportional to fast-ion density) vs major radius from the vertical FIDA views for the two discharges shown in Fig. 1. Solid lines: *FIDASIM* code predictions using classical fast-ion transport. Symbols: actual measurements. Dashed line: *FIDASIM* prediction for the high-q_{min} case after applying uniform fast-ion diffusion above the classical level. The FIDA spectra are summed over wavelengths of 650.5–652.7 nm, which corresponds to energies along the line-of-sight of 25–68 keV.

diffusion profile. A value of 1.3 m^2/s was chosen because this makes the computed stored energy and neutron rate approximately match the experimental values. This value improves the match between prediction and experiment, although no attempt was made to find a fast-ion diffusion profile that might make a best fit to the FIDA data.

For the $q_{min} \approx 2$ case, if only the inferred absorbed NBI power (i.e., what is left after applying an ad-hoc fast-ion diffusion) is included in the calculation, then H_{89P} rises from 1.8 to 2.2. This again implies that enhanced fast ion transport is the primary reason for lower normalized confinement at $q_{min} > 2$. Power balance analysis with the inferred absorbed power finds that the thermal diffusivities do not differ significantly between the high- and low-q_{min} cases. Thus, under the presumption that NBI power is redistributed by Alfvénic modes this particular high-q_{min} plasma has thermal transport similar to the low-q_{min} case. It is possible that any expected increase in thermal transport with q is being offset by a decrease due to lower shear.[26] But without significantly improved thermal transport the $q_{min} \approx 2$ case has $H_{89P} < 2$ because the fast-ions are not classically confined.

Degraded fast-ion confinement in the presence of enhanced AE activity is reproducibly observed by all fast-ion diagnostics that are sensitive to the co-passing portion of velocity space. Figure 4 compares classical and measured signals for the stored energy, volume-averaged neutron rate, and vertically viewing FIDA diagnostic in several quasi-stationary discharges with $q_{95} = 5$–12. The classically predicted neutron signals are derived from a zero-dimensional prediction of the beam-plasma collision rate,[27] and the FIDA data and the fast-ion stored energy points are from the carefully analyzed discharges of Ref. 28. When there are many coherent AEs, the classical prediction overestimates the measured signals. The four discharges with a neutron overestimate greater than 100% are all at the lowest current (0.5–0.65 MA) in the group and they have quite strong AEs at $\rho = 0.6$–0.7.

Local fluctuation diagnostics show that the AE activity occurs throughout much of the plasma volume. Figure 5 shows electron cyclotron emission (ECE)[31] measurements of the AE profile for three coherent modes in a quasi-stationary discharge with $\beta_N = 2.8$, $q_{min} = 2.5$, $q_{95} = 6.9$, and $H_{89P} = 1.4$. The mode at 113 kHz is located near the q_{min} radius, which is at a normalized minor radius of $\rho = 0.37$ in this discharge; this is probably a reverse-shear AE.[32] The mode at 137 kHz is localized near the top of the H-mode pedestal. The mode at 153 kHz is a global mode, probably a TAE.

Both the MHD code NOVA-K[37,38] and the gyrokinetic code GYRO[33] predict AE instability for high-q_{min} plasmas. For example, GYRO was used to predict the eigenfunctions of AEs in the pair of discharges shown in Fig. 1. The calculations were performed in the range $\rho = 0.2$–0.8. The fast-ion pressure profiles supplied as inputs are those that result after any fast-ion diffusion needed to match the measured total stored energy is applied, i.e., for the high-q_{min} case the fast-ion pressure is lower than the classical prediction. Figure 6 compares the electrostatic potential of the most unstable eigenfunction for an $n = 4$ mode. The case with $q_{min} = 2$ has the potential for AEs extending out to higher radius. Figure 6(b) compares the growth rates for a range of n. The high-q_{min} case has larger growth rate than the low-q_{min} case for $n = 2$–13. If the classically predicted fast ion pressure is used for the high-q_{min} case, then the predicted growth rates are significantly higher. (The low-q_{min} case fast ion pressure is already approximately classical).

Theoretically, the many modes cause fast-ion transport through resonance overlap.[29,30] Figure 7 illustrates this last point by comparing phase space diagrams for a pair of steady-state scenario plasmas at high- and low-q_{min}. In both, the possible fast-ion orbits are gray symbols. Black symbols show where the NBI sources used in the discharge actually populate phase space with fast ions. Red symbols denote possible fast ion orbits that can resonate with the various AEs that were observed in the discharge. Where red and

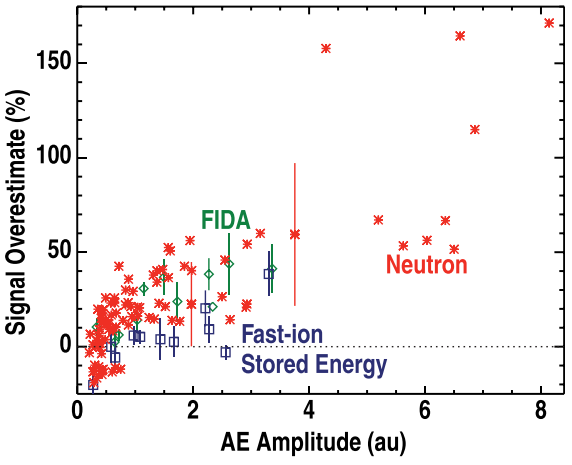

FIG. 4. Signal overestimate vs AE amplitude for quasi-stationary discharges from the 2013 and 2014 experimental campaigns. The overestimate is defined as (classical prediction—signal)/signal. The AE amplitude is the time average of coherent modes in the TAE band inferred from interferometer signals. Representative error bars associated with the 15% uncertainty in the absolute neutron calibration are shown.

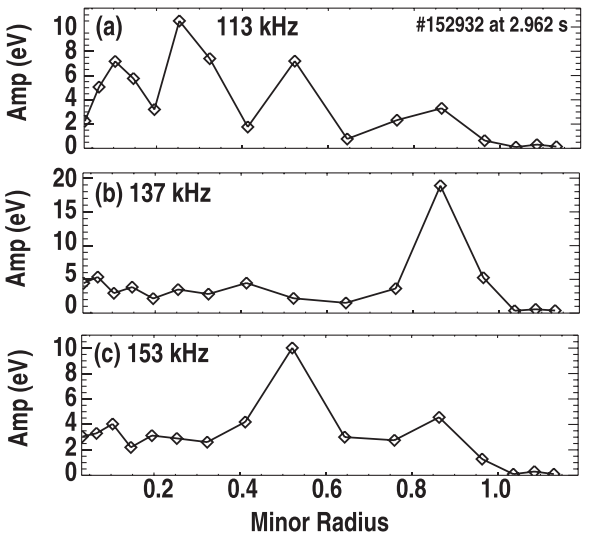

FIG. 5. ECE fluctuation amplitude vs ρ for three coherent modes in a discharge with degraded fast-ion and global confinement.

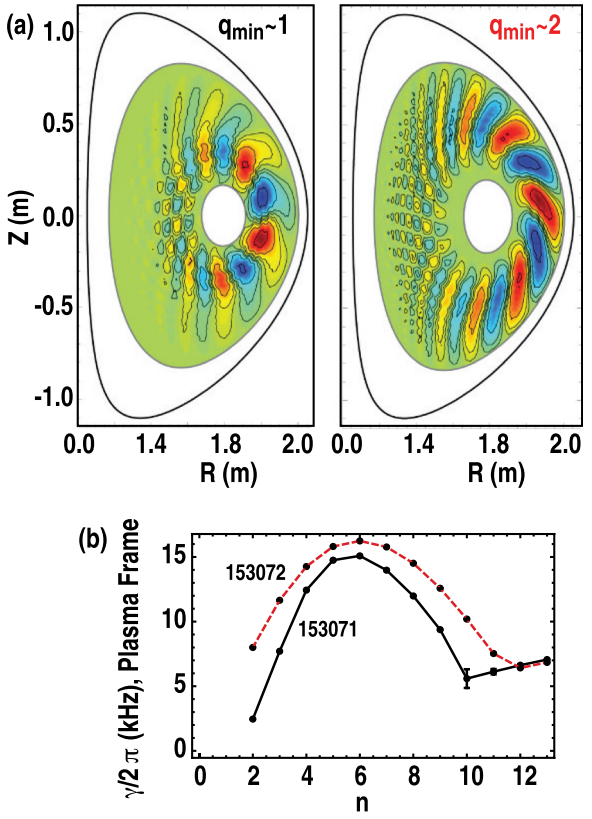

FIG. 6. GYRO eigenvalue solver code predictions for (a) the electrostatic potential of the most unstable eigenfunction for an $n = 4$ mode; and (b) growth rates for a range of toroidal mode numbers.

black symbols overlap—i.e., where actual fast-ion orbits are capable of resonating with observed modes—there is the possibility for fast ion redistribution to other parts of phase space, including to loss orbits. While the case with $q_{min} = 1$ has little overlap, the case with $q_{min} = 2$ has substantial overlap.

In summary, the standard high-q_{min} steady-state scenario is observed to have lower than expected global energy confinement, substantial AE activity, and a deficit of confined fast ions compared to classical predictions. The negations of these statements are true for similar low-q_{min} plasmas. AE stability calculations confirm that the high-q_{min} plasmas have greater potential for instability and fast-ion transport than the low-q_{min} plasmas. This implies an important question: is high-q_{min} by itself necessarily bad for fast-ion transport and global energy confinement? Section III will show that the answer to this question is "no".

III. HIGH q_{min} WITH HIGH β_P

Very high q_{min} in the range of 3–5 has been sustained with $H_{89P} \geq 2$ in the DIII-D "High-β_P" regime[34–36] that is used to prepare for long-pulse operation on superconducting tokamaks like EAST. Fully noninductive plasmas sustained by 70%–80% bootstrap current fraction and the 20%–30% NBI + ECCD have been produced in the following parameter ranges: β_N = 3–4, β_P = 3–4, β_T = 1.5%–2.5%, q_{95} = 11–12.5, I_P = 600–700 kA, and $B_T = 2$ T. The

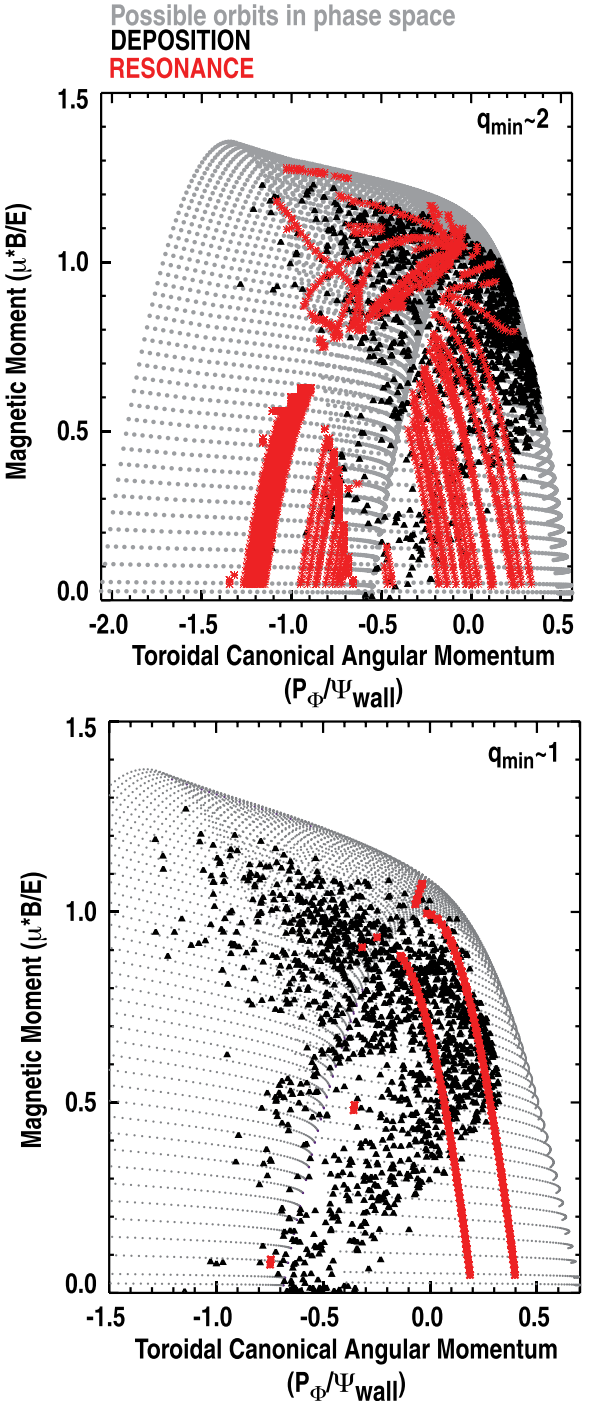

FIG. 7. Plots of possible fast-ion orbits in phase space for (a) a high-q_{min} discharge and (b) a low-q_{min} discharge. Gray points: all possible orbits. Black points: actual fast-ion orbits at the time of deposition produced by the NBI combinations used in the discharge. Red points: orbits computed to be resonant with observed AEs.

line–density through the magnetic axis is typically in the range 5.5–6.5 × 10^{19} m^{-3}. Successful shots with both thermal and total-energy confinement at or above levels expected for H-mode[19] (i.e., $H_{98P} \geq 1$ and $H_{89P} \geq 2$) have either a high radius ($\rho \approx 0.7$) transport barrier or infrequent edge localized modes (ELMs) and a high average pedestal pressure. Figure 8 shows time traces and profiles for an example High-β_P discharge.

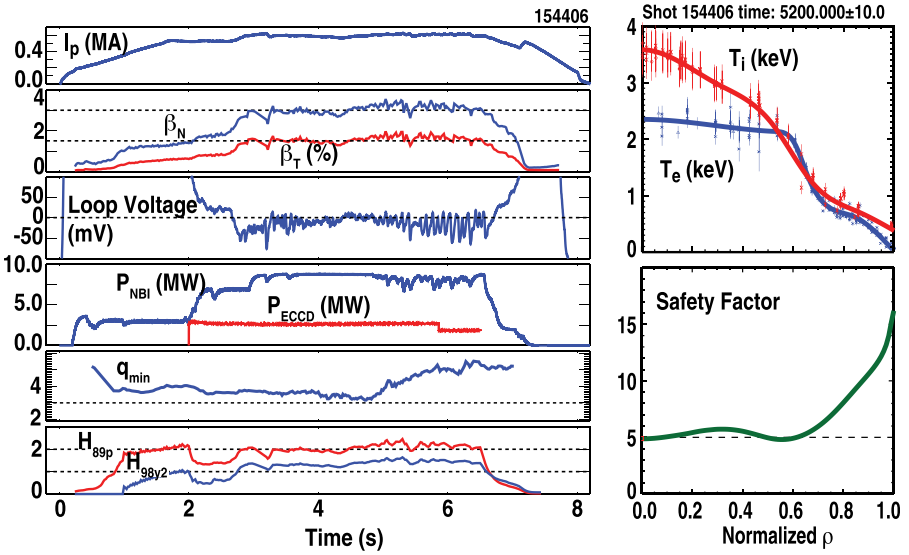

FIG. 8. Features of a high-β_P discharge. Left: time histories of (from top to bottom) I_P, β_N, and β_T, surface loop voltage, NBI and ECCD power, q_{min}, H_{89P}, and H_{98y2}. Right: radial profiles of electron and ion temperature and q at t = 5200 ms.

High-β_P plasmas with $H_{89P} \geq 2$ have inferred fast-ion transport near the classical level. Figure 9 compares a standard high-q_{min} case and a high-β_P case. Whereas the standard case has $q_{min} \approx 2.4$, $H_{89P} \approx 1.8$ H, and a ~15% stored energy overestimate, the high-β_P case has $H_{89P} \approx 2.1$, and a stored energy overestimate of ~3% with almost double the value of q_{min}. Figure 10 shows the FIDA profile acquired between 3900–6000 ms during ELM-free phases in the same high-β_P discharge. (The absence of ELMs facilitates accurate FIDA measurements despite the relatively high density of this discharge.) Within experimental uncertainty, the FIDA, neutron, and stored energy measurements are all consistent with classical theory. The high-β_P discharges demonstrate that very high values of q_{min} in the range of 3–5 do not invariably result in enhanced fast-ion transport or lower than expected global energy confinement. In both high-q_{min} regimes the strongest AEs observed are usually TAEs, and NOVA code[37,38] analysis (Fig. 11) of a pair of discharges finds that the core TAE gap structure inside of $\rho \approx 0.5$ is much wider for the standard high-q_{min} case than the high-β_P case. In the former case, NOVA predicts a plethora of radially extended core TAEs that are minimally damped, while in the latter case the TAE gap only widens a similar amount outside of $\rho \approx 0.5$. Measurements of density and temperature fluctuations associated with TAEs are in qualitative agreement with these predictions. Figure 12 compares profiles of the electron temperature fluctuation frequency-spectrum measured by the electron cyclotron emission diagnostic. The standard high-q_{min} plasma has many more coherent modes inside of $\rho \approx 0.5$ than the high-β_P case, which has strong modes around 60 and 70 kHz only outside of $\rho \approx 0.6$. Since in both cases the fast-ion profile is peaked on-axis, AEs near the magnetic axis are more likely to cause enhanced fast-ion transport than AEs at large radius.

The drive for core AEs is lower in high-β_P plasmas than in standard high-q_{min} plasmas because the former have a shorter slowing-down time and therefore a lower classically predicted $\nabla\beta_{fast}$ [Figs. 13(a) and 13(b)]. This is consistent with recent work[39] that suggests that the strength of AE activity in L-mode, high-q_{min} plasmas has a critical-$\nabla\beta_{fast}$

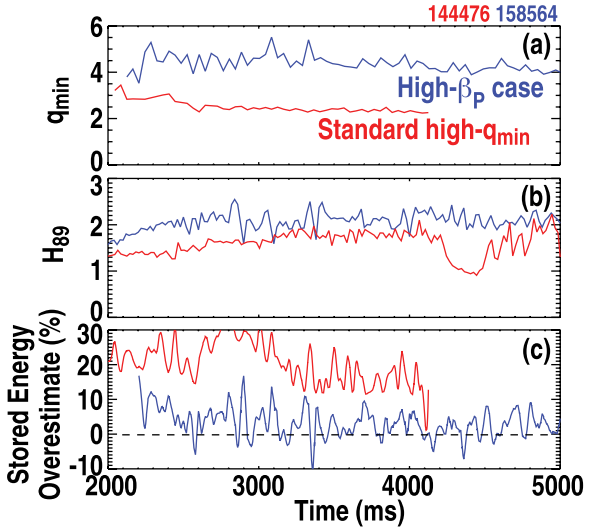

FIG. 9. Time traces of q_{min}, H_{89P}, and stored energy overestimate for a standard high-q_{min} discharge and a high-β_P discharge.

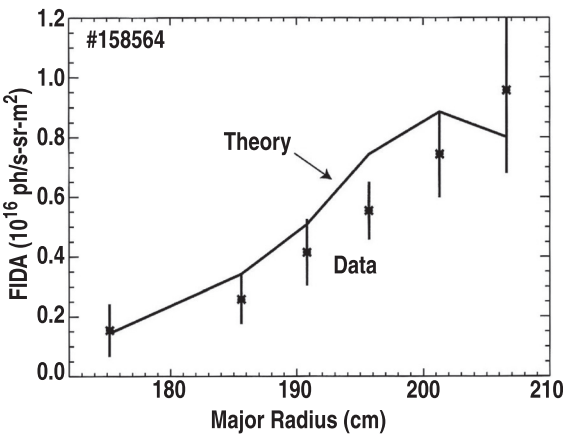

FIG. 10. FIDA profile from the oblique view that is sensitive to co-passing fast ions.[42] The error bars represent the temporal variation of the ratio of experimental-to-theoretical values. The theoretical prediction assumes classical fast ions. The FIDA spectra are summed over wavelengths of 650.5–652.7 nm.

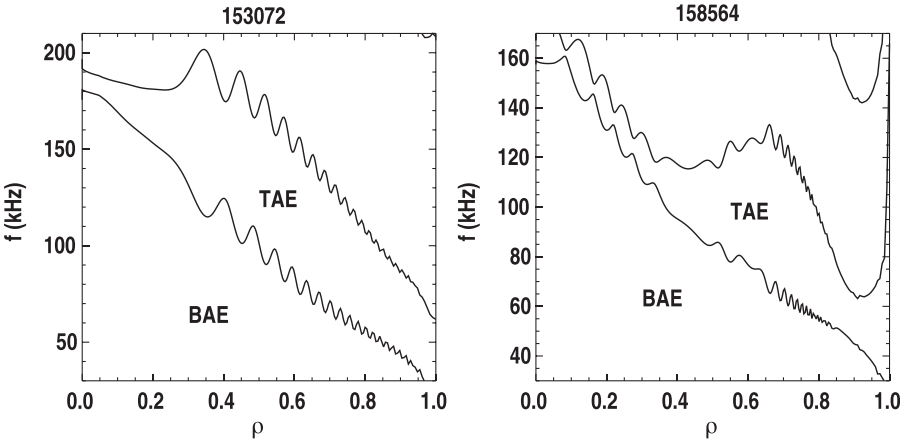

FIG. 11. *NOVA* code calculations of the TAE gap profiles for a standard high-q_{min} discharge (153 072, left) and a high-β_P discharge (158 564, right).

dependence whereby the modes and fast-ion transport increase quickly above a certain value of $\nabla\beta_{fast}$. This produces stiff fast-ion transport and limits the actual fast-ion profile peaking (i.e., actual profiles show less peaking than classically predicted profiles). In the high-β_P cases, the shorter slowing-down times across the whole profile result from higher density and lower electron temperature. Profiles of these are usually "step-like," i.e., relatively flat inside a transport barrier, rapidly changing at the barrier, and then flat again out to the H-mode pedestal barrier. Between the transport barriers, the very short slowing-down time should be more effective at thermalizing fast ions before they can be expelled from the plasma relative to plasmas without this feature.

Many observations made in high-β_P plasmas lead to the conclusion that these operate very close to a critical fast-ion gradient for enhanced transport. Reducing the density in these plasmas results in an increase in AE activity, lower confinement time and lower achievable β_N. In the example shown in Fig. 14, only the density is changed between two consecutive discharges, from a maximum of about $6.5 \times 10^{19}\,m^{-3}$ to about $5 \times 10^{19}\,m^{-3}$. Lowering the density increased the slowing-down time, raised the maximum classically predicted fast-ion gradient by 50%–60%, increased the number and amplitude of AEs, and reduced H_{89P} to less than 2. Figure 15 shows another discharge in which the line-density was again about $5 \times 10^{19}\,m^{-3}$. As before, strong AE activity was observed. In the middle of the high-β_N phase, the total NBI power was stepped down by about 32%. After this change, the classically predicted maximum in $\nabla\beta_{fast}$ is reduced, the interferometer shows a reduction in AE amplitude, the stored energy overestimate falls from 5%–10% to close to 0 (i.e., the classical level), and remarkably, β_N remains approximately constant at 3. These observations are consistent with the NBI power reduction causing a relaxation of $\nabla\beta_{fast}$ to below a critical value and subsequently a reduction in fast-ion transport. Considering this case backwards in

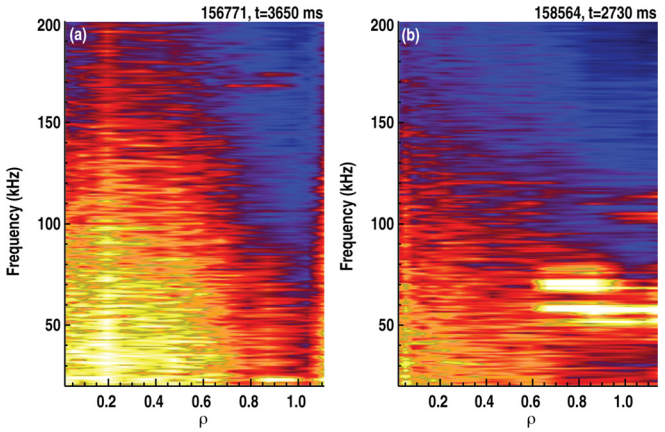

FIG. 12. Cross power spectra profiles of electron temperature fluctuations measured by the electron cyclotron emission diagnostic. Left: a standard high-q_{min} case. Right: a high-β_P case.

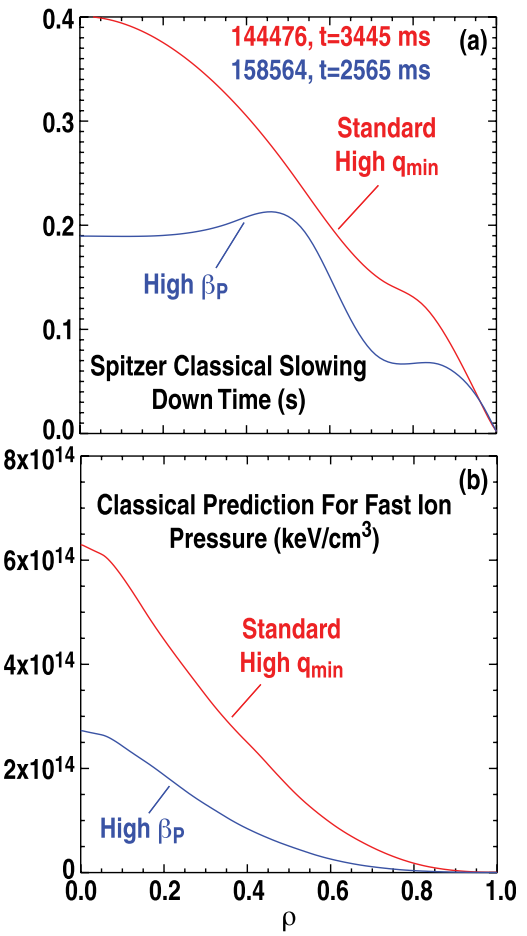

FIG. 13. (a) Profiles of the Spitzer classical slowing down time $[t_s \equiv (2\pi/m_e)^{1/2}T_e^{3/2}/m_b A_d$, where $A_d \equiv n_e e^4 \ln(\Lambda)/2\pi\varepsilon_0^2 m_b^2]$, and (b) the classically predicted fast-ion pressure.

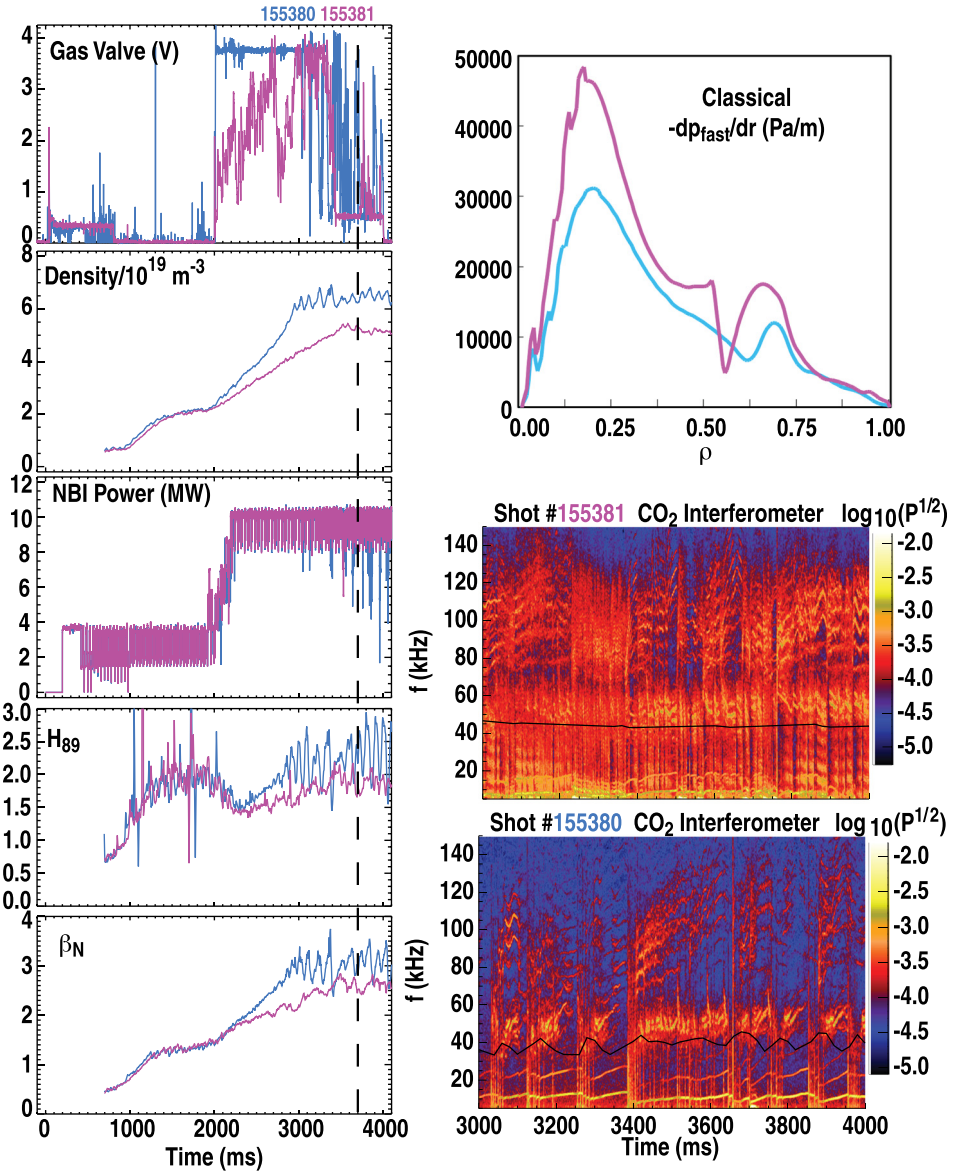

FIG. 14. Left: Time traces of gas valve injection voltage, density, NBI power, H_{89P}, and β_N for two high-β_P discharges. Right: profiles of the classically predicted fast-ion pressure gradient near t = 3700 ms, and time traces of cross-power density fluctuation spectra.

time (i.e., as if it were an NBI power step-up) shows that the effectiveness of NBI power to increase β_N falls rapidly once the critical gradient has been reached. Through variation of density and NBI power the classically predicted $\nabla\beta_{fast}$ can be varied. Figure 16 shows a compilation of data from different times in three high-β_P discharges. The AE amplitude and stored energy overestimate increase with increasing $\nabla\beta_{fast}$ while H_{89P} decreases. These observations are consistent with the picture of fast-ion transport increasing with $\nabla\beta_{fast}$.

The interplay between fast-ion transport and thermal transport is noteworthy for its complexity in high-β_P discharges. A correlation is observed between classical or nearly classical fast-ion confinement and the existence of either a transport barrier near $\rho = 0.7$ or a transport barrier near $\rho = 0.5$ with a higher pedestal pressure. Conversely, lower density discharges with enhanced fast-ion transport and lower H_{89P} do not have internal transport barriers or higher pedestals. Figures 17 and 18 compare pairs of discharges to illustrate these points. In Fig. 17, both discharges had the same density feedback target waveform, but in one case more NBI power was used at early times resulting in an earlier L-to-H-mode transition time and higher q_{min}. Once in H-mode, the density of both discharges followed the same trajectory until about t = 3 s when the higher-q_{min} case developed a transport barrier in all channels at $\rho = 0.7$. After this time, the density and temperature inside the barrier rose to higher values than what was observed in the discharge without a barrier. But, the slowing-down-time profiles and classically predicted fast-ion pressure profiles did not change significantly. Thus the stored energy overestimate remained near 10% until after the NBI power was reduced at about t = 4.3 s. In this case, the transport barrier apparently formed while the fast-ion transport was still higher than classical. The increase in thermal stored energy brought about by the barrier compensated for the enhanced fast-ion transport and achieved higher confinement and β_N than the case without a barrier.

The example in Fig. 18 compares the low-H_{89P} discharge from Fig. 17 to a case programmed to have higher density for the entire discharge. The higher density case is inferred to have nearly classical fast-ion transport for the entire high-β_N phase of the discharge. After about t = 2.3 s

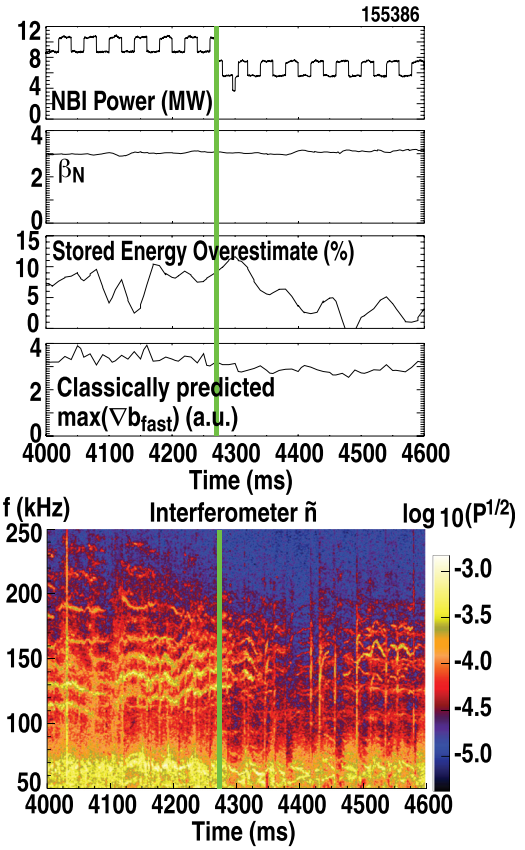

FIG. 15. High-β_P discharge time traces of NBI power, β_N, stored energy overestimate, maximum classically predicted gradient in β_{fast}, and density fluctuation spectra.

this discharge obtains a higher average pedestal pressure, β_N, and H_{89P}. The higher average pedestal pressure is a result of an unsteady, but unusually long (~100–500 ms) ELM period. This coexists with a transport barrier near $\rho = 0.5$ that is somewhat narrower and shorter than the barriers observed at $\rho = 0.7$ in other discharges. In this case, it appears that the attainment of nearly classical fast-ion confinement precedes and possibly contributes to the formation of the high pedestal and internal transport barrier by more complete transfer of heat to the thermal plasma.

The comparisons in Figs. 17 and 18 show improved thermal confinement can either push the global energy confinement time back up to expected H-mode levels (i.e., $H_{89P} \geq 2$) despite enhanced fast-ion transport, or a mode of better thermal confinement (e.g., internal transport barrier or higher pedestal) can result from having classical fast-ion transport. In either case, better thermal confinement reduces the required NBI power to obtain a target β_N, which helps to reduce the drive for AE modes.

In summary, the high-β_P operating scenario shows that high-q_{min} plasmas can have classical fast-ion confinement and good global energy confinement if $\nabla\beta_{fast}$ is kept low in the core to avoid strong AE activity there. This is caused by a relatively low and flat slowing-down time profile inside $\rho \sim 0.5$. There may be other ways to control the slowing-down time and fast-ion profiles to minimize AE activity and achieve good performance. These are discussed in Sec. IV.

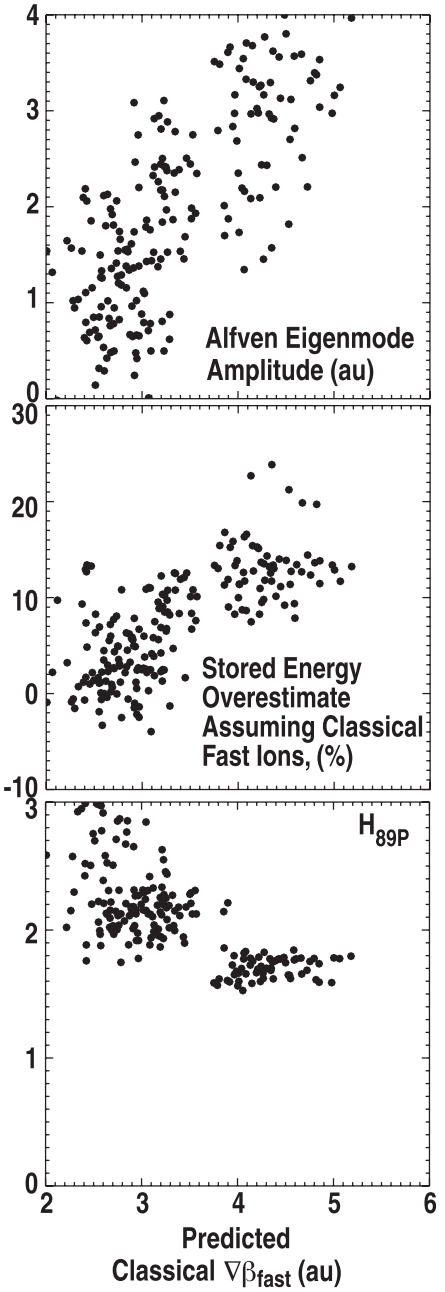

FIG. 16. From top to bottom: Average AE amplitude, stored energy overestimate, and H_{89P} versus classically predicted gradient in β_{fast}. Data is taken from three high-β_P discharges.

IV. FUTURE OUTLOOK

On DIII-D, achieving higher β_N in high-q_{min} plasmas with reactor-relevant q_{95} will require improved control of fast-ion modes. The L-mode studies in Ref. 39 showing that moving the same amount of NBI power from on- to off-axis reduces AE activity suggests that moving more NBI power from on- to off-axis may help in a high-q_{min}, high-β_N scenario. Presently, ~1/3 of the co-I_P NBI power is injected off-axis in these scenarios, but a planned upgrade will increase this to ~2/3. This will enable further lowering of the fast-ion gradient near the axis, which will reduce the drive for AEs there. The high-β_P regime demonstrates cases where some mode of improved thermal confinement can either partially

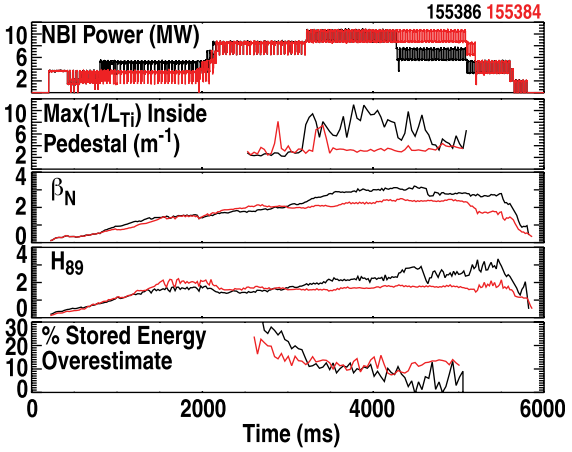

FIG. 17. Comparison of discharges showing the effects of an internal transport barrier. From top to bottom: NBI power, maximum inverse gradient scale length of the ion temperature inside the pedestal (large values indicate the presence of a barrier), β_N, H_{89P}, and stored energy overestimate versus time. The no-ITB case is in red and with-ITB case is in black.

compensate for enhanced fast-ion transport, or permit classical fast-ion transport by lowering the NBI power requirement. In both cases, the normalized confinement is at or above the expected level for an H-mode plasma. Therefore, future experiments should seek to identify and optimize potentially useful regimes of improved thermal confinement. The most likely modes to be compatible with high-q_{min} are a high-radius transport barrier or a "super-H-mode" pedestal.[40]

A third lesson from the present experiments is that future experiments should seek to replace NBI heating with rf-electron heating. This will lower the drive for AEs and avoid the issue of reducing fast-ion confinement. This option is actually well aligned with future burning plasma reactors, which, unlike the experiments described here, will have chiefly electron heating, low input torque, and isotropic rather than anisotropic fast ions. To this end, the DIII-D program has plans for a significant increase in ECH power and will test a novel high-harmonic fast wave or "helicon" system for off-axis heating and current drive. Lastly, in DIII-D

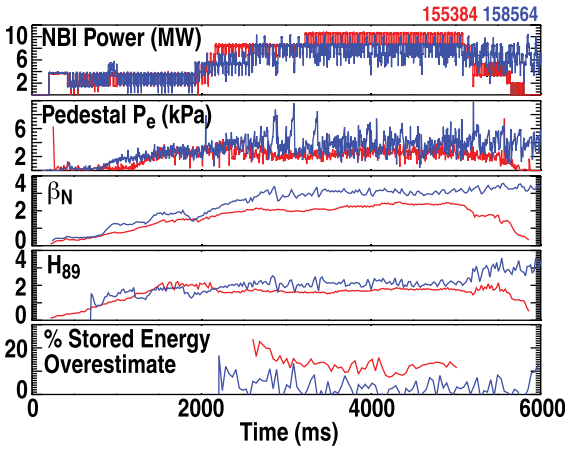

FIG. 18. Comparison of discharges showing the effects of a nearly classical fast-ion transport and higher average pedestal pressure. From top to bottom: NBI power, electron pedestal pressure, β_N, H_{89P}, and stored energy overestimate versus time.

and elsewhere there have been observations of direct impacts on reverse-shear AEs and TAEs by the careful application of ECH. For example, modulation between ECH on- and off-axis has been shown to turn TAEs on and off at the same rate that is faster than a slowing down time.[41] These results are not fully understood and from low-β_N plasmas, but their existence encourages continued exploration of novel AE-control methods.

It was beyond the scope of the present paper to try to predict fast-ion confinement in next-generation steady state burning plasmas based on existing DIII-D results. But a few important dimensionless parameters can be compared to get some sense of how conditions will be different in ITER, for example. Taking parameters from a model $q_{min} > 2$ steady-state scenario for ITER[5] shows that it will have a mix of both more and less favorable conditions than DIII-D for fast-ion confinement. The analysis in this paper has focused mostly on the drive for AEs and resulting fast-ion transport. The quotient $\beta_{fast}/\beta_{thermal}$ serves as a proxy for the ratio of AE drive to damping. In the DIII-D high-q_{min} plasmas with $q_{95} = 5$–7 all having enhanced fast-ion transport, $\beta_{fast}/\beta_{thermal} = 0.2$–0.4. The high-$\beta_P$ plasmas having approximately classical fast-ion transport have $\beta_{fast}/\beta_{thermal} = 0.15 - 0.35$. The predicted ITER plasma from Ref. 5 would have $\beta_{fast}/\beta_{thermal} = 0.15$. This is at the low end of the DIII-D high-β_P range, and therefore, this is favorable for ITER. Next, the much larger size of ITER compared to DIII-D means that the ratio of the fast-ion orbit to machine size ρ_{fast}/a is much lower in ITER: 0.015 for beam ions and 0.02 for alphas compared to 0.03–0.04 in the DIII-D experiments. Therefore, the ability of AEs to move fast-ions all the way to the edge of the plasma is less in ITER. But ITER will have many more fast-ions that are capable of resonating with various AEs than DIII-D: the ratio of (on-axis) parallel fast-ion speed to Alfvén speed v_{fast}/v_A is 0.3–0.45 in DIII-D but about 0.64 for beam ions in ITER and over 1 for alpha particles. Thus additional experiments and modeling are needed to improve confidence in predictions of fast-ion confinement in high-q_{min} scenarios in ITER.

V. SUMMARY

Recent DIII-D steady-state scenario experiments have shown the importance of optimizing the current density and fast-ion pressure profiles to minimize AE instability and fast-ion transport. High-β_N operation is dominated by co-I_P neutral beam injection heating, and therefore confined fast ions can make up a significant fraction of the total stored energy. Many experiments have had q_{95} in the range 5–7, because this corresponds to a value that would produce a reasonable level of fusion gain in a next-step reactor. Also, to maximize the externally driven noninductive current the line-density is often kept below $\sim 5 \times 10^{19}$ m^{-3}. With these conditions, an increase of fast-ion transport above classically predicted levels occurs when q_{min} is raised from just above 1 to just above 2. This results in 20%–30% lower global energy confinement time at the higher value of q_{min}. Taking the inferred lower absorbed NBI heating power into account, the thermal ion and electron diffusivities are found to be similar for both values of q_{min}.

A high-β_P, high-q_{min} scenario developed in a different regime is useful for clarifying the physics underlying enhanced fast-ion transport, and also for demonstrating paths to recovering good global energy confinement. When higher q_{95} (i.e., lower I_P) and line-density above $\sim 5 \times 10^{19}\,m^{-3}$ are used, this results in high-β_P plasmas ($\beta_P = 3$–4) that have $H_{89P} > 2$ and classical fast-ion transport. Classical fast-ion transport is evident even with $q_{min} \approx 5$ and ~8–10 MW of NBI power because higher density and lower temperature lead to shorter slowing-down times and a smaller fast-ion pressure gradient. Compared to standard high-q_{min} plasmas ($q_{95} = 5$–7), the high-β_P plasmas have a narrower TAE gap structure near the magnetic axis and observed AEs are usually only outside $\rho = 0.5$. Good high-β_P plasmas operate just below but close to a critical fast-ion gradient for increased AE activity. The thermal plasma has either a high-radius transport barrier or a high average pedestal pressure, and these help to reduce the required NBI power and fast-ion gradient. These observations suggest that improved global energy confinement in standard high-q_{min} plasmas might be achieved by using planned heating and current drive upgrades to broaden the NBI heating profile and further optimize thermal transport at high radius.

ACKNOWLEDGMENTS

This material was based upon work supported in part by the U.S. Department of Energy, Office of Science, Office of Fusion Energy Sciences, using the DIII-D National Fusion Facility, a DOE Office of Science user facility, under Award Nos. DE-FC02-04ER54698, DE-AC52-07NA27344, SC-G903402, DE-AC02-09CH11466, DE-AC05-00OR22725, and DE-FG02-04ER54761. DIII-D data shown in this paper can be obtained in digital format by following the links at https://fusion.gat.com/global/D3D_DMP.

[1]J. L. Luxon, Fusion Sci. Technol. **48**, 828 (2005).
[2]M. Murakami, M. R. Wade, C. M. Greenfield, T. C. Luce, J. R. Ferron, H. E. St John, J. C. DeBoo, W. W. Heidbrink, Y. Luo, M. A. Makowski, T. H. Osborne, C. C. Petty, P. A. Politzer, S. L. Allen, M. E. Austin, K. H. Burrell, T. A. Casper, E. J. Doyle, A. M. Garofalo, P. Gohil, I. A. Gorelov, R. J. Groebner, A. W. Hyatt, R. J. Jayakumar, K. Kajiwara, C. E. Kessel, J. E. Kinsey, R. J. La Haye, L. L. Lao, A. W. Leonard, J. Lohr, T. W. Petrie, R. I. Pinsker, R. Prater, T. L. Rhodes, A. C. C. Sips, G. M. Staebler, T. S. Taylor, M. A. Van Zeeland, G. Wang, W. P. West, L. Zeng, and the DIII-D Team, Phys. Plasmas **13**, 056106 (2006)
[3]ITER Physics Expert Group on Energetic Particles, Heating, and Current Drive and ITER Physics Basis Editors, Nucl. Fusion **39**, 2471 (1999).
[4]W. W. Heidbrink and G. J. Sadler, Nucl. Fusion **34**, 535 (1994).
[5]M. Murakami, J. M. Park, G. Giruzzi, J. Garcia, P. Bonoli, R. V. Budny, E. J. Doyle, A. Fukuyama, N. Hayashi, M. Honda, A. Hubbard, S. Ide, F. Imbeaux, E. F. Jaeger, T. C. Luce, Y.-S. Na, T. Oikawa, T. H. Osborne, V. Parail, A. Polevoi, R. Prater, A. C. C. Sips, J. Snipes, H. E. St. John, P. B. Snyder, I. Voitsekhovitch, and ITPA/Integrated Operation Scenario Group, Nucl. Fusion **51**, 103006 (2011).
[6]F. M. Poli, C. E. Kessel, P. T. Bonoli, D. B. Batchelor, R. W. Harvey, and P. B. Snyder, Nucl. Fusion **54**, 073007 (2014).
[7]A. M. Garofalo, V. S. Chan, J. M. Canik, M. E. Sawan, M. Choi, D. A. Humphreys, L. L. Lao, R. Prater, P. C. Stangeby, H. E. St. John, T. S. Taylor, A. D. Turnbull, and C. P. C. Wong, Nucl. Fusion **54**, 073015 (2014).
[8]C. E. Kessel, T. K. Mau, S. C. Jardin, and F. Najmabadi, Fusion Eng. Des. **80**, 63 (2006).
[9]T. S. Taylor, H. St. John, A. D. Turnbull, Y. R. Lin-Liu, K. H. Burrell, V. Chan, M. S. Chu, J. R. Ferron, L. L. Lao, R. J. La Haye, E. A. Lazarus, R. L. Miller, P. A. Politzer, D. P. Schissel, and E. J. Strait, Plasma Phys. Control. Fusion **36**, B229 (1994).
[10]T. C. Luce, Fusion Sci. Technol. **48**, 1212 (2005).
[11]A. D. Turnbull, F. Yasseen, A. Roy, O. Sauter, W. A. Cooper, S. Nicli, and F. Troyon, Nucl. Fusion **29**, 629 (1989).
[12]C. M. Greenfield, D. P. Schissel, B. W. Stallard, E. A. Lazarus, G. A. Navratil, K. H. Burrell, T. A. Casper, J. C. DeBoo, E. J. Doyle, R. J. Fonck, C. B. Forest, P. Gophil, R. J. Groebner, M. Jakubowski, L. L. Lao, M. Murakami, C. C. Petty, C. L. Rettig, T. L. Rhodes, B. W. Rice, H. E. St. John, G. M. Staebler, E. J. Strait, T. S. Taylor, A. D. Turnbull, K. L. Tritz, R. E. Waltz, and DIII-D Team, Phys. Plasmas **4**, 1596 (1997).
[13]M. Greenwald, Plasma Phys. Control. Fusion **44**, R27 (2002).
[14]P. N. Yushmanov, T. Takizuka, K. S. Riedel, O. J. W. F. Karduan, J. G. Cordey, S. M. Kaye, and D. E. Post, Nucl. Fusion **30**, 1999 (1990).
[15]J. R. Ferron, C. T. Holcomb, T. C. Luce, J. M. Park, P. A. Politzer, F. Turco, W. W. Heidbrink, E. J. Doyle, J. M. Hanson, A. W. Hyatt, Y. In, R. J. La Haye, M. J. Lanctot, M. Okabayashi, T. W. Petrie, C. C. Petty, and L. Zeng, Phys. Plasmas **20**, 092504 (2013).
[16]B. Wan, J. Li, H. Guo, Y. Liang, G. Xu, and Xianzhu Gong for the EAST Team and International Collaborators, Nucl. Fusion **53**, 104006 (2013).
[17]E. J. Strait for the DIII-D Team, Nucl. Fusion **49**, 104008 (2009).
[18]C. C. Petty, *Proceedings of the 25th IAEA Fusion Energy Conference, St. Petersburg, Russian Federation*, 2014, paper no. PPC/P2-36. Available at http://www-pub.iaea.org/MTCD/Meetings/PDFplus/2014/cn221/cn221ConferenceProgrammeAndAbstracts.pdf.
[19]ITER Physics Groups on Confinement and Transport and Confinement Modeling and Database, ITER Physics Basis Editors, and ITER EDA, Nucl. Fusion **39**, 2175 (1999).
[20]C. Z. Cheng and M. S. Chance, Phys. Fluids **29**, 3695 (1986).
[21]L. L. Lao, H. St. John, R. D. Stambaugh, A. G. Kellman, and W. Pfeiffer, Nucl. Fusion **25**, 1611 (1985).
[22]H. E. St. John, T. S. Taylor, Y. R. Lin-Liu, and A. D. Turnbull, in *Proceedings of the 15th International Conference on Plasma Physics and Controlled Nuclear Research*, Seville, Spain, 1994 (IAEA, Vienna, 1995), Vol. 3, p. 603.
[23]A. Pankin, D. McCune, R. Andre, G. Bateman, and A. Kritz, Comput. Phys. Commun. **159**, 157 (2004).
[24]W. W. Heidbrink, Rev. Sci. Instrum. **81**, 10D727 (2010).
[25]W. W. Heidbrink, D. Liu, Y. Luo, E. Ruskov, and B. Geiger, Commun. Comput. Phys. **10**, 716 (2011).
[26]C. C. Petty, T. C. Luce, D. R. Baker, B. Ballet, T. N. Carlstrom, J. G. Cordey, J. C. DeBoo, P. Gohil, R. J. Groebner, B. W. Rice, D. M. Thomas, M. R. Wade, and R. E. Waltz, Phys. Plasmas **5**, 1695 (1998).
[27]W. W. Heidbrink, P. L. Taylor, and J. A. Phillips, Rev. Sci. Instrum. **68**, 536 (1997).
[28]W. W. Heidbrink, J. R. Ferron, C. T. Holcomb, M. A. Van Zeeland, Xi Chen, C. M. Collins, A. Garofalo, X. Gong, B. A. Grierson, M. Podesta, L. Stagner, and Y. Zhu, Plasma Phys. Control. Fusion **56**, 095030 (2014).
[29]R. Nazikian, N. N. Gorelenkov, B. Alper, H. L. Berk, D. Borba, R. V. Budny, G. Y. Fu, W. W. Heidbrink, G. J. Kramer, M. A. Makowski, S. D. Pinches, S. E. Sharapov, W. M. Solomon, E. J. Strait, R. B. White, M. A. Van Zeeland, and JET-EFDA contributors, Phys. Plasmas **15**, 056107 (2008).
[30]M. A. Van Zeeland, W. W. Heidbrink, R. K. Fisher, M. García Muñoz, G. J. Kramer, D. C. Pace, R. B. White, S. Aekaeslompolo, M. E. Austin, J. E. Boom, I. G. J. Classen, S. da Graça, B. Geiger, M. Gorelenkova, N. N. Gorelenkov, A. W. Hyatt, N. Luhmann, M. Maraschek, G. R. McKee, R. A. Moyer, C. M. Muscatello, R. Nazikian, H. Park, S. Sharapov, W. Suttrop, G. Tardini, B. J. Tobias, Y. B. Zhu, and DIII-D and ASDEX Upgrade Teams, Phys. Plasmas **18**, 056114 (2011).
[31]M. E. Austin and J. Lohr, Rev. Sci. Instrum. **74**, 1457 (2003).
[32]Y. Kusama, H. Kimura, T. Ozeki, M. Saigusa, G. J. Kramer, T. Oikawa, S. Moriyama, M. Nemoto, T. Fujita, K. Tobita, G. Y. Fu, R. Nazikian, and C. Z. Cheng, Nucl. Fusion **38**, 1215 (1998).
[33]J. Candy and R. Waltz, J. Comput. Phys. **186**, 545 (2003).
[34]P. A. Politzer, A. W. Hyatt, T. C. Luce, F. W. Perkins, R. Prater, A. D. Turnbull, D. P. Brennan, J. R. Ferron, C. M. Greenfield, J. Jayakumar, R. J. La Haye, C. C. Petty, and M. R. Wade, Nucl. Fusion **45**, 417 (2005).
[35]A. G. Garofalo, *Proceedings of the 25th IAEA Fusion Energy Conf., St. Petersburg, Russian Federation*, 2014, paper no. PPC/P2-31. Available at http://www-pub.iaea.org/iaeameetings/46091/25th-Fusion-Energy-Conference-FEC-2014.

[36]X. Gong, *Proceedings of the 25th IAEA Fusion Energy Conf., St. Petersburg, Russian Federation*, 2014, paper no. EX/P2-39. Available at http://www-pub.iaea.org/iaeameetings/46091/25th-Fusion-Energy-Conference-FEC-2014.
[37]C. Z. Cheng and M. S. Chance, J. Comput. Phys. **71**, 124 (1987).
[38]N. N. Gorelenkov, C. Z. Cheng, and G. Y. Fu, Phys. Plasmas **6**, 2802 (1999).
[39]W. W. Heidbrink, M. A. Van Zeeland, M. E. Austin, E. M. Bass, K. Ghantous, N. N. Gorelenkov, B. A. Grierson, D. A. Spong, and B. J. Tobias, Nucl. Fusion **53**, 093006 (2013).
[40]W. M. Solomon, P. B. Snyder, K. H. Burrell, M. E. Fenstermacher, A. M. Garofalo, B. A. Grierson, A. Loarte, G. R. McKee, R. Nazikian, and T. H. Osborne, Phys. Rev. Lett. **113**, 135001 (2014).
[41]M. A. Van Zeeland, W. W. Heidbrink, R. Nazikian, M. E. Austin, C. Z. Cheng, M. S. Chu, N. N. Gorelenkov, C. T. Holcomb, A. W. Hyatt, G. J. Kramer, J. Lohr, G. R. McKee, C. C. Petty, R. Prater, W. M. Solomon, and D. A. Spong, Nucl. Fusion **49**, 065003 (2009).
[42]C. M. Muscatello *et al.*, Rev. Sci. Instrum. **81**, 10D316 (2010).